High-Mobility Air-Stable Solution-Shear-Processed n-Channel Organic Transistors Based on Core-Chlorinated Naphthalene Diimides

*Wen-Ya Lee, Joon Hak Oh, Sabin-Lucian Suraru, Wen-Chang Chen, Frank Würthner, and Zhenan Bao**

High charge carrier mobility solution-processed n-channel organic thin-film transistors (OTFTs) based on core-chlorinated naphthalene tetracarboxylic diimides (NDIs) with fluoroalkyl chains are demonstrated. These OTFTs were prepared through a solution shearing method. Core-chlorination of NDIs not only increases the electron mobilities of OTFTs, but also enhances their air stability, since the chlorination in the NDI core lowers the lowest unoccupied molecular orbital (LUMO) levels. The air-stability of dichlorinated NDI was better than that of the tetrachlorinated NDIs, presumably due to the fact that dichlorinated NDIs have a denser packing of the fluoroalkyl chains and less grain boundaries on the surface, reducing the invasion pathway of ambient oxygen and moisture. The devices of dichlorinated NDIs exhibit good OTFT performance, even after storage in air for one and a half months. Charge transport anisotropy is observed from the dichlorinated NDI. A dichlorinated NDI with $-CH_2C_3F_7$ side chains reveals high mobilities of up to 0.22 and 0.57 $cm^2 V^{-1} s^{-1}$ in parallel and perpendicular direction, respectively, with regard to the shearing direction. This mobility anisotropy is related to the grain morphology. In addition, we find that the solution-shearing deposition affects the molecular orientation in the crystalline thin films and lowers the d(001)-spacing (the out-of-plane interlayer spacing), compared to the vapor-deposited thin films. Core-chlorinated NDI derivatives are found to be highly suitable for n-channel active materials in low-cost solution-processed organic electronics.

1. Introduction

Organic electronics, including organic thin-film transistors (OTFTs),[1,2] organic light-emitting diode (OLED),[3] and organic photovoltaics (OPVs),[4] offer an attractive alternative to conventional inorganic electronics owing to their potential in low-cost, large-area fabrication and mechanical flexibility of organic materials. Recently, much progress has been made in p-type organic semiconductors,[1,2,5–9] whereas the development of n-channel counterparts still lags behind that of the p-type materials,[5–10] because ambient oxygen and moisture act as electron traps, significantly reducing the performance of many n-channel organic materials in air. To date, a few n-channel small molecules and polymers exhibit high-performance air-stable OTFT performance in air.[5,6,11–18] Both p-type and n-channel semiconductors are required for the fabrication of low-power-consumption complementary metal oxide semiconductor (CMOS) circuits. Therefore, the development of high-performance air-stable solution processable n-channel organic semiconductors is of great importance.

Naphthalene diimides (NDIs) are among the most promising n-channel candidates for OTFTs due to their high electron affinity and large π-orbital overlap in the solid state,[13,19,20] However, the electrical performance of n-alkyl NDIs degrades rapidly in air. To improve the air-stability, two molecular designs of NDI were commonly employed: (i) introduction of fluorinated substituents[13,20] at the imide nitrogen and (ii) addition of strong

Dr. W.-Y. Lee, Dr. J. H. Oh, Prof. Z. Bao
Department of Chemical Engineering
Stanford University
381 North-South Mall, Stanford, CA 94305, USA
E-mail: zbao@stanford.edu
Dr. W.-Y. Lee, Prof. W.-C. Chen
Department of Chemical Engineering
National Taiwan University
Institute of Polymer Science and Engineering
National Taiwan University
Taipei 106, Taiwan
Dr. J. H. Oh
School of Nano-Bioscience and Chemical Engineering and KIER-UNIST Advanced Center for Energy
Ulsan National Institute of Science and Technology
Ulsan 689-798, Korea
S. Suraru, Prof. F. Würthner
Institut für Organische Chemie and Röntgen Research Center for Complex Material Systems
Universität Würzburg
Am Hubland, 97074 Würzburg, Germany

DOI: 10.1002/adfm.201101606

electron-withdrawing groups at the NDI core.[5,21,22] The introduction of fluorinated substituents at the imide nitrogen is known to allow the formation of densely packed fluorocarbon chains to provide a kinetic barrier and prevent the intrusion of ambient oxidants.[13,20] Shukla et al. reported a remarkably high electron mobility of approximately 6 $cm^2 V^{-1} s^{-1}$ from cycloalkyl-NDIs, but the mobility in air degraded significantly.[23] Katz group reported that NDIs substituted with fluorinated phenylethyl groups[20] showed a long-term air-stable electron mobility of 0.18 $cm^2 V^{-1} s^{-1}$ after exposure to air for 1 month. The ambient stability is also improved by adding strong electron-withdrawing groups such as cyano,[5] chlorine,[24,25] and fluorine,[24,26] in the core region, since these electron-withdrawing groups lower the LUMO levels significantly, leading to enhancing their resistivity to ambient oxidations. Recently, we have demonstrated that the film morphology and grain boundaries also affect the air stability of the n-channel molecules significantly, even for n-channel semiconductors with low-lying LUMO levels. This indicates that the interplay between kinetic and energetic factors play an important role for the air-stability.[27]

Most high-performance n-channel OTFT devices were obtained from vapor-deposited thin films. However, OTFT devices fabricated by solution processing commonly exhibited lower performance due to the poor film quality of the solution-processed films. Currently, the fabrication of high-performance air-stable solution-processed n-channel OTFT is still a challenge. Recently, Yan and coworkers reported that an air-stable solution-processable n-channel polymer P(NDI2OD-T2), consisting of NDI and bithiophene moieties, exhibited a remarkable electron mobility of 0.85 $cm^2 V^{-1} s^{-1}$ from the specific polymeric dielectrics (ActivInk D2200, polyolefin-polyacrylate) and top-gate bottom-contact configuration,[28] while the polymer only showed electron mobilities of 0.06 $cm^2 V^{-1} s^{-1}$ from the OTFTs based on a conventional SiO_2 substrate and bottom-gate top-contact configuration.[29] The difference of the performance of this n-channel polymer is due to the result of using an electron-trap-tree dielectric layer, and the top-gate bottom-contact configuration, which reduces the damage caused by gold electrode deposition on organic semiconductor thin films. With a SiO_2 dielectric and bottom-gate top-contact configuration, Gao et al. reported the best performance of 0.51 $cm^2 V^{-1} s^{-1}$ from the solution processed OTFTs of core-expanded NDIs fused with 2-(1,3-dithiol-2-ylidene) malonitrile.[18] Furthermore, these core-expanded NDIs exhibited a dramatically enhanced mobility of 1.2 $cm^2 V^{-1} s^{-1}$ on the bottom-gate bottom-contact OTFTs through modifying pentafluorobenzene thiol on Au electrodes.[17] These results depict a possibility for excellent solution-processed n-channel organic semiconductors through the modification of NDI cores.

Despite the challenges in controlling film crystallinity and uniformity, solution processing approach is important for realizing low-cost large-area organic electronics. Several solution processing techniques, such as spin coating,[19] drop casting,[13,14,30] zone casting,[31,32] solution shearing[30,33,34] and printing,[35–37] have been employed for organic semiconductors. Among these techniques, the solution-shearing deposition (SS)[30,33,34] is a simple and rapid tool for screening solution-processed OTFTs, especially for small molecule semiconductors. This method can easily control thin film thickness, uniformity and crystallization by tuning the solution concentrations, shearing rates, solvents and substrate temperatures (T_{sub}). Furthermore, SS impacts crystallization direction and molecular orientation under appropriate conditions. The aligned nature of SS films exhibited a higher mobilities in many cases than those of the equivalent devices fabricated from drop-casting and spin-coating methods.[30,34]

Here we report the electrical performance of solution-processed OTFTs prepared from four core-chlorinated NDI derivatives with fluorinated alkyl chains. The chemical structures of the NDI molecules are shown in **Figure 1**. Recently, we reported the synthesis of these core-chlorinated NDIs and the performance of their vacuum-processed OTFTs.[38] The NDIs with two chlorine substituents exhibited high field-effect mobilities up to 1.43 $cm^2 V^{-1} s^{-1}$ that are attributed to the very close π-plane distance (3.3–3.4 Å), a large π-stack overlap (slipping angle ca. 62°) and high density in the crystalline state (2.046–2.091 gcm^{-3}).[38] Unlike tetrachlorinated PDIs that show a significantly twisted backbone, tetrachlorinated NDIs have a planar π-plane backbone with a dihedral angle of only about 7°, leading to a slip-stacked face-to-face packing and high mobility up to 0.44 $cm^2 V^{-1} s^{-1}$.[38] The introduction of fluorinated alkyl chains induces a dense molecular packing for improved ambient stability without disturbing the planarity of π–π orbital overlap. The chlorination on the core region lowers the LUMO energy levels of the NDI derivatives, compared to the unsubstituted core. As compared to fluoro-functionalized molecules, chloro-functionalized molecules showed a smaller band gap and an enhanced electron mobility, presumably due to the delocalization of the π-electrons into empty 3*d* orbitals of the chlorine substituents, while the fluorine atoms do not have such accessible orbitals.[24] Cyclic voltammetry measurements revealed the LUMO levels of –3.72, –4.01, –4.13 and –4.01 eV, for **1**, **2**, **3** and **4**, respectively. The LUMO level of the NDI was shifted significantly from –3.72 to –4.13 eV after substitution with four chlorine atoms in the NDI core.[38] The advantages for the lower

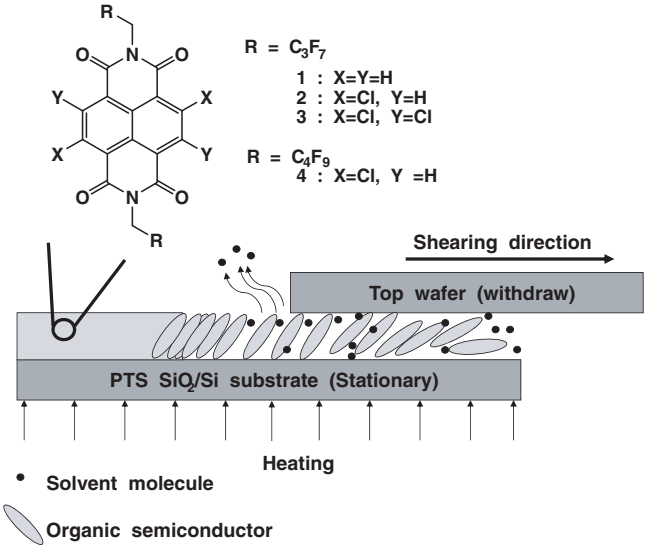

Figure 1. Schematic illustration of solution shearing method, and chemical structures of the naphthalene diimides (NDIs) used in this study.

LUMO levels are to decrease the Schottky barrier for electron injection, and to make electron charge carriers less sensitive to the trapping by ambient oxygen and moisture in air. The chlorinated NDIs have a good solubility in chlorinated solvents such as chloroform and 1,2-dichlorobenzene, indicating that these NDIs have the advantage for the solution processing. To investigate the performance of the solution processed OTFTs, solution shearing and spin coating were employed for the fabrication of devices based on the chlorinated NDIs. The schematic setup of the SS deposition is shown in Figure 1. All the solution-processed OTFTs were fabricated in air. The SS OTFTs of dichlorinated NDI **2** showed excellent electron mobilities up to 0.57 $cm^2 V^{-1} s^{-1}$, which is comparable with the performance (0.86 $cm^2 V^{-1} s^{-1}$) of its vacuum-processed devices. The devices of dichlorinated NDIs still exhibited high performance, even after storage in air for one and a half month. This depicts a promising future for excellent air-stable solution-processed n-channel organic semiconductors by the chlorination of NDI cores. The charge transporting, morphology, air-stability and molecular packing of these solution-processed chlorinated NDIs were investigated in this study.

2. Results and Discussion

The solution-shearing deposition method was employed for the fabrication of OTFTs. We also prepared spin-coated devices to compare with the performance of solution-sheared devices. Figure 1 illustrates the basic concept of the SS process. A small amount of organic semiconductor solution was placed on phenyltrichlorosilane (PTS)-treated SiO_2/Si substrates. The modification of PTS can facilitate the wetting of the NDI solutions on SiO_2/Si substrate, and passivates the silanol groups on the surface.[30] The substrate temperatures ranged between 60 (108 °C) and 80% (144 °C) of the boiling-point of the solvent used. Pulling the top wafer against the stationary wafer exerted a shearing force while crystallization started at the exposed region and proceeded parallel to the shearing direction.[30] In this study, a low shearing speed of 0.086 mm s^{-1} was found to allow slow crystallization of the films for optimal OTFT performance. A high boiling-point solvent, *o*-dichlorobenzene (ODCB) (b.p. = 178 °C), resulted in films with full substrate coverage and relatively better uniformity. All NDI molecules showed good solubility in ODCB. The saturated solubilities of the NDIs in ODCB at room temperature are 36, 8, 21 and 17 mg ml^{-1} for **1**, **2**, **3** and **4**, respectively. The chlorinated NDIs showed a lower solubility compared to the unsubstituted parent NDI, probably due to the fact that high polarizability of chlorine atoms and a Van-der-Waals radius (175 pm) identical to the extension of an aromatic π cloud, thus leading to enhanced the intermolecular dipole-induced interaction between the chlorinated NDI molecules. In the SS deposition, the temperatures of the substrates and the boiling-point of the solvent of the molecules are critical factors for the film quality and morphology.

The morphologies of the solution-sheared films were studied by atomic force microscopy (AFM). **Figure 2** shows atomic force microscopy (AFM) images of the SS films under a deposition temperature of 126 °C (70% b. p. of DCB). Figure 2(a) shows a ribbon-like morphology of the SS film from **1**. The

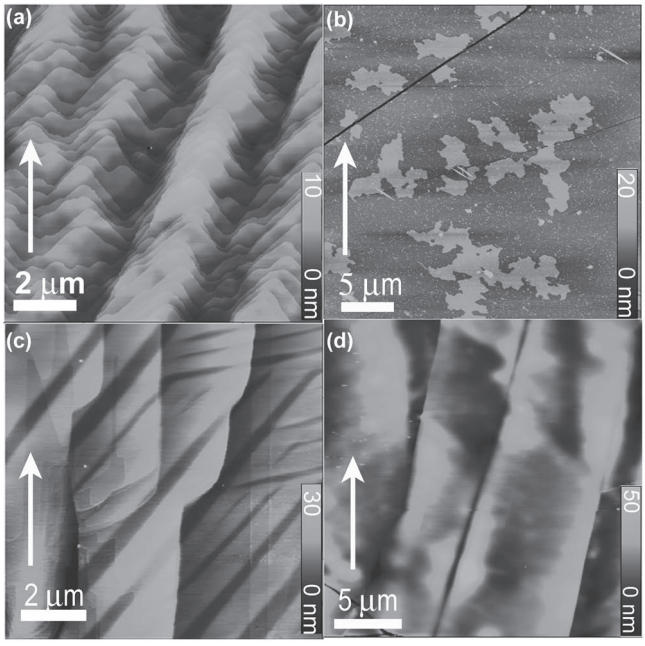

Figure 2. Tapping-mode AFM characterizations of the SS thin films. The AFM topography (top) images of **1** (a), **2** (b), **3** (c), and **4** (d) thin films, respectively. Those thin films were deposited through the solution-sheared process. The shearing direction is marked with a white arrow.

films of **1** were rough with peak-to-valley distance as high as 8.1 nm. Figure 2(c) shows an AFM topography image of the SS thin film from **3**. It formed elongated large grains (also see Figure S1). Figure 2(b) and 2(d) show terraced morphologies of **2** and **4**, respectively. The SS **2** thin film exhibited a terraced structure consisting of large grains with unidirectional cracks. These cracks are mostly 45° from the shearing direction. The film of **2** appeared quite smooth except for a few terraces with their edges along the shearing direction. SS film of **4** showed a terraced morphology similar to that of **2**, but a rougher surface (root-mean-square (RMS) roughness: 8.21 nm) than that of **2** (RMS roughness: 2.46 nm). Note that the AFM images of **1** and **3** show more visible boundaries than **2** and **4**. Such morphologies with many boundaries are undesirable for charge transport, because they typically lead to a low mobility as seen later.

The OTFT performance obtained from these NDI derivatives is summarized in **Table 1**, where the average values were obtained from at least four devices for each condition. Except for a few cases (for details, see Table 1), all the devices had the current flow direction along the shearing direction. The electron mobility in the saturation regime was calculated from the slope of the square root of drain-to-source current $(I_{DS})^{1/2}$ vs. the gate voltage (V_G).[2] As shown in Table 1, the optimized average mobilities of **1**, **2**, **3** and **4** were 0.016, 0.17, 0.022 and 0.05 $cm^2 V^{-1} s^{-1}$, respectively, and the on/off ratios were 10^4 to 10^5. Dichlorinated NDIs exhibited higher mobilities than the unsubstituted and tetrachlorinated NDIs, consistent with the trend observed for the performance of their corresponding vacuum-processed devices. Part of this was attributed to the fact that chlorine atoms provide empty 3d orbitals for the delocalization of π-electrons, and the dichlorinated NDI molecules

Table 1. Summary of electrical properties of NDI SS OTFTs.

Compound	Solvent	T_{sub} (°C)	Maximum mobility ($cm^2 V^{-1} s^{-1}$)	mobility ($cm^2 V^{-1} s^{-1}$)	Average on/off	V_t (V)
1	ODCB	108	2.63×10^{-2}	$(1.64 \pm 0.58) \times 10^{-2}$	7.94×10^4	14 ± 8
	ODCB	126	1.15×10^{-2}	$(9.89 \pm 3.62) \times 10^{-3}$	6.98×10^4	10 ± 6
	ODCB	144	4.38×10^{-3}	$(2.32 \pm 2.07) \times 10^{-3}$	6.90×10^4	8 ± 5
	CHCl3*	rt[a)]	2.68×10^{-5}	$(1.86 \pm 0.85 \times 10^{-5}$	7.57×10^2	-2 ± 10
2	ODCB	108	3.65×10^{-2}	$(1.68 \pm 0.78) \times 10^{-2}$	2.90×10^4	-27 ± 11
	ODCB	126	2.16×10^{-1} (5.67×10^{-1})[b)]	$(1.73 \pm 0.60) \times 10^{-1}$ (($4.08 \pm 1.48) \times 10^{-1}$)[b)]	2.65×10^5 (1.27×10^6)[b)]	-23 ± 10 (-11 ± 8)[b)]
	ODCB	144	1.79×10^{-1}	$(1.00 \pm 0.60) \times 10^{-1}$	1.75×10^5	-13 ± 10
	$CHCl_3$*	rt[a)]	6.33×10^{-4}	$(4.09 \pm 1.58) \times 10^{-4}$	2.47×10^2	-60 ± 9
3	ODCB	108	1.70×10^{-2}	$(8.20 \pm 5.33) \times 10^{-3}$	2.92×10^5	4 ± 8
	ODCB	126	3.99×10^{-2}	$(2.20 \pm 1.20) \times 10^{-2}$	1.03×10^5	2 ± 3
	ODCB	144	2.96×10^{-2}	$(1.65 \pm 1.14) \times 10^{-2}$	1.20×10^5	16 ± 1
	CHCl3*	rt[a)]	5.61×10^{-5}	$(2.44 \pm 0.74) \times 10^{-5}$	4.22×10^2	-8 ± 3
4	ODCB	108	6.78×10^{-4}	$(3.62 \pm 1.95) \times 10^{-4}$	2.79×10^3	-1 ± 20
	ODCB	126	6.50×10^{-2}	$(4.50 \pm 2.16) \times 10^{-2}$	1.92×10^5	-36 ± 13
	ODCB	144	1.37×10^{-2}	$(9.29 \pm 5.54) \times 10^{-3}$	1.03×10^5	-22 ± 12
	$CHCl_3$*	rt[a)]	1.01×10^{-3}	$(5.62 \pm 3.18) \times 10^{-4}$	4.70×10^2	-5 ± 6

[a)]rt means room temperature. Devices denoted with * were fabricated by spin coating; [b)]The electric properties in the parentheses were estimated in the vertical device, which charge transport was vertical with the shearing direction.

give the closest π–π stack packing, increasing the π–π orbital overlap.[38] This might also originate from the morphological effects. As shown in the AFM images, dichloro-substituted NDIs, **2** and **4**, formed terraced morphologies in the films with larger and smoother grains compared to **1** and **3**. Furthermore, core-chlorinated NDIs have lower LUMO levels making them less susceptible to electron traps compared to the parent compound **1**. However, in the case of **3**, the four chlorine atoms on the core induce significant steric hindrance on the adjacent chlorine atoms and distort the NDI π-conjugated core. Consequently, the π–π interaction between the NDI cores may be reduced and gives rise to a lower TFT performance for **3**. The grain morphology and the degree of chlorination of **4** are similar to those of **2**, but the OTFT performance of **4** is almost an order of magnitude lower than that of **2**. It may be due to the rough grain boundaries. We found that the RMS roughness of **4** (8.21 nm) was much higher than that of **2** (2.46 nm). In addition, some deep gaps and cracks were also observed on the surface of **4** which may act as barriers for charge transport.

To investigate the influence of the substrate temperature (T_{sub}) on the performance of the SS OTFTs, we prepared SS OTFTs at various T_{sub} (from 60 to 80% of the b.p. of ODCB). The T_{sub} plays an important role in the performance of vapor-deposited OTFT made through the vapor deposition by critically affecting the growth of the crystals.[6,12,39] For solution-sheared depositions, T_{sub} affects evaporation rates of solvents and the solubilities of small molecules. As shown in Table 1, the performance of OTFTs is sensitive to T_{sub}. The SS OTFTs of **1** exhibited a reduced mobility as T_{sub} increased due to the formation of many long cracks developed for a few days after deposition. In contrast, the SS OTFTs of the chlorinated NDI derivatives showed the best mobilities of 0.17 $cm^2 V^{-1} s^{-1}$ for **2**, 0.022 $cm^2 V^{-1} s^{-1}$ for **3** and 0.045 $cm^2 V^{-1} s^{-1}$ for **4** at an elevated temperature of 126 °C. Moreover, AFM characterizations revealed fewer cracks in the thin films of **2** at 126 °C than the films prepared at other temperatures. The AFM topography and phase images of **2** deposited at various temperatures are shown in **Figure 3**(a–e). When **2** was deposited at 108 °C (60% b.p. of ODCB), the film consisted of large terraces with height 1.60 ± 0.13 nm, close to one molecular layer thickness (the *d(001)*-spacing from X-ray diffraction (XRD) analysis: 19.28 Å), and had many unidirectional cracks and small grains on the surface as shown in Figure 3(a) and 3(d). When the T_{sub} was increased to 126 °C, the films showed less grain boundaries and larger grains. The higher T_{sub} of 144 °C led to more cracks on the surface after cooling due to the mismatch of the thermal expansion coefficients between the small molecule and the SiO_2/Si substrate.[6] Furthermore, the T_{sub} higher than 144 °C resulted in a fast evaporation rate of ODCB and a short deposition time for the film formation, leading to a decreased mobility. The spin-coated devices have also been tested for a comparison, as shown in Table 1. The mobility of the spin-coated OTFTs was consistently lower than that of solution-sheared devices. This is attributed to the fact that the crystal structure tends to be ill-defined in the spin-coated films. Note that the spin-coated dichloro-substituted NDI **2** and **4** devices also gave higher mobility than the NDI **1** and the tetrachloro-substituted NDI **3**.

In the above TFTs, the current flow direction was parallel to the shearing direction. To investigate the charge transport anisotropy, we also prepared devices containing the source (S)-drain (D) electrodes with different orientations where the current flow direction was controlled to be 0°, 22.5°, 45°, or 90° with regard to the shearing direction. The *I*–*V* curves and the electrical properties are shown in **Figure 4** and **Table 2**, respectively. The perpendicular-orientation (90°) device exhibited a much higher average mobility of 0.41 $cm^2 V^{-1} s^{-1}$ and the maximum mobility of up to 0.57 $cm^2 V^{-1} s^{-1}$, which is higher than that of the parallel-orientation (0°) devices, and with a high average on/off ratio of 1.27×10^6. The device in 45° orientation exhibited the lowest average mobility of 0.056 $cm^2 V^{-1} s^{-1}$, approximately one third of the mobility of the parallel-orientation devices. The difference in mobility is possibly related to the cracks in the films and the difference in the molecular orientation in the solid state packing.[40] The cracks are mostly at about 45° from the shearing direction. They are presumably along a certain crystallographic plane. As mentioned in the AFM characterizations above, the morphology of **2** exhibits a longer grain length in the horizontal than that in the vertical direction, resulting in a higher mobility from the perpendicular-orientation devices compared to parallel-orientation devices. Furthermore,

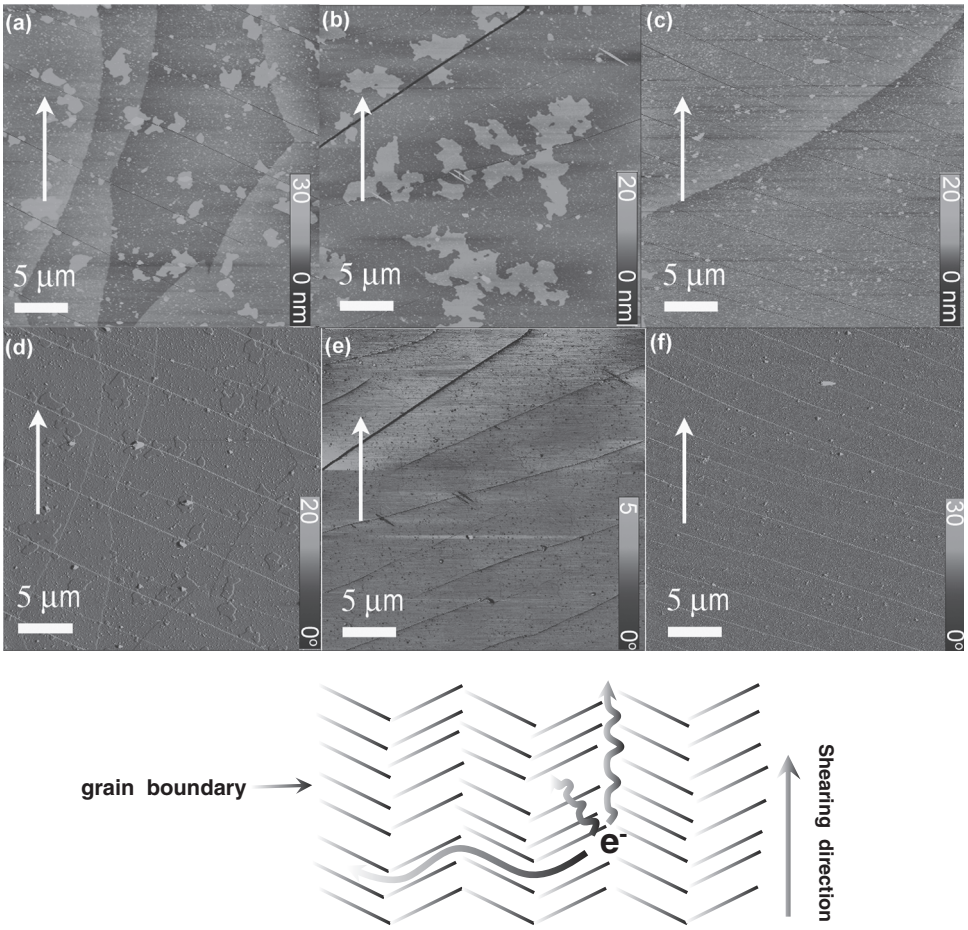

Figure 3. The topography (a–c) and phase images (d,e) of **2** deposited at the various temperatures: 108 (a and d), 126 (b and e) and 144 °C (c and f). The bottom image is a schematic model for electron transport anisotropy in the terraced morphology of **2**.

the grain width along 45° is shorter than that in the parallel and perpendicular, resulting in a lower performance in this direction. These OTFT performances confirm our hypothesis that the anisotropy in the grain-boundary between source and drain electrodes dominantly affects the charge carrier mobilities, leading to the charge transport anisotropy. It should be noted that we did not observe any difference in mobility when measuring in the perpendicular direction for NDIs 1, 3, and 4. We observed the SS **2** films composed of crystalline ribbons showing strong birefringence from the cross-polarized optical images of the films (Figure S1 in Supporting Information). The schematic explanation concept of charge transport anisotropy is illustrated in the bottom of Figure 3. It is worth noting that **2** revealed the high electron mobility of up to 0.57 $cm^2\ V^{-1}\ s^{-1}$ which is among the highest values reported from solution-processed air-stable n-channel OTFTs by employing the conventional SiO_2 dielectrics and the same device configuration. This mobility of the SS **2** device is close to that of vapor-deposited devices (0.86 $cm^2\ V^{-1}\ s^{-1}$), indicating that the SS process is capable of providing a simple and effective way for the fabrication of high-performance solution-processed OTFTs.

The performance for **2** with the shorter fluoroalkyl side chains is better than that for **4** with one more CF_2 unit in the fluoroalkyl chains, i.e. C_5F_9 chains at the imide nitrogens. Similar trend has been observed for tetrachlorinated NDIs. To investigate the influence of the lengths of fluoroalkyl chains, we measured the OTFT performance of the tetrachlorinated NDI homologue with five carbons through the SS deposition. This material showed a slightly lower average electron mobility of $3.25 \times 10^{-2}\ cm^2\ V^{-1}\ s^{-1}$ at the T_{sub} of 126 °C, as compared to that of **3** having C_4F_7 in the fluoroalkyl chains. OTFTs made from chlorinated NDIs with shorter side chains showed higher mobilities. The trend obtained from SS thin films is opposite to the trend of the OTFTs prepared from vapor-deposited thin films.[38] This implies that the different lengths of the imide side chain groups of the NDI molecules may lead to a different molecular packing in solution-processed thin films, compared to their vapor deposited counterpart.

For n-channel TFTs, air-stability is a typical concern due to trapping by oxygen in ambient air. Therefore, air-stability of the devices was monitored by measuring mobility (μ), on/off ratio (I_{on}/I_{off}), and threshold voltage (V_t) as a function of time, as shown in **Figure 5**. All the electrical properties for the air-stability measurement were carried out for the parallel-direction devices. The fluctuation of the above observed parameters correlated well with the relative humidity (RH) and has been

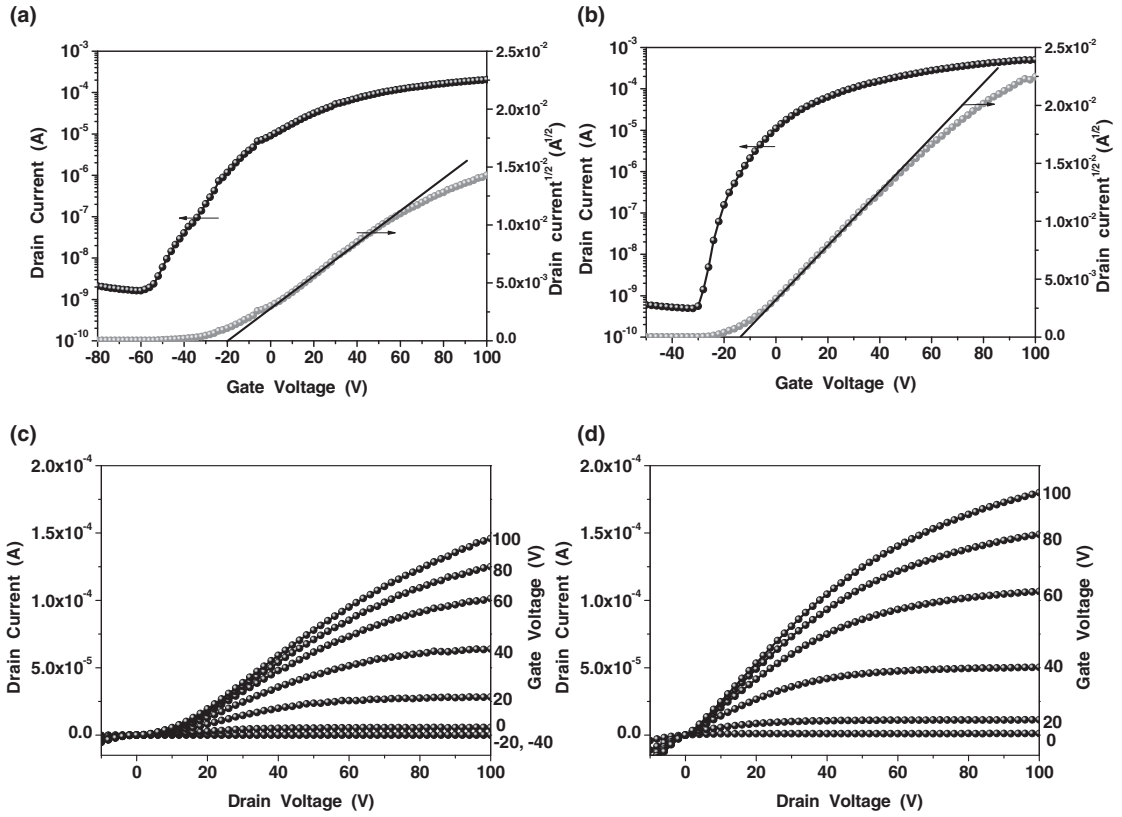

Figure 4. The transfer (a,b) and output (c,d) characteristics of OTFTs of **2** in the parallel orientation (a,c) and the perpendicular orientation (b,d), showing the charge-transport anisotropy.

Table 2. Summary of the OTFT devices of **2** patterned in the various directions.

Angle(°)[a]	Maximum mobility ($cm^2 V^{-1} s^{-1}$)	Average mobility ($cm^2 V^{-1} s^{-1}$)	Average on/off	Average V_t (V)
0	2.16×10^{-1}	$(1.73 \pm 0.60) \times 10^{-1}$	2.65×10^5	-23 ± 10
22.5	1.66×10^{-1}	$(1.52 \pm 0.16) \times 10^{-1}$	4.34×10^5	-8 ± 5
45	9.82×10^{-2}	$(5.63 \pm 3.71) \times 10^{-2}$	7.13×10^4	-2 ± 11
90	5.67×10^{-1}	$(4.08 \pm 1.48) \times 10^{-1}$	1.27×10^6	-11 ± 8

[a]The angle is defined as the angle between the current flowing direction and clockwise from the shearing direction as indicated by the white arrows in Figure S1.

commonly observed.[41] The average mobility of **1**, **2**, **3** and **4** only decreased slightly from 0.016, 0.17, 0.022 and 0.045 to 0.01, 0.11, 0.0086 and 0.019 $cm^2 V^{-1} s^{-1}$, respectively, after exposure to air for one and half months. In the vacuum-processed OTFTs, the air-stability of dichlorinated NDIs was superior to that of tetrachlorinated NDIs, despite of their higher LUMO levels.[38] In SS OTFTs, **2** also showed the better air stability than **3**, regardless of their LUMO levels. This fact is presumably related to the fact that the SS thin films of dichlrinated NDIs have larger and well-defined grains and prevent the intrusion of oxygen and moisture more efficiently, compared to the SS thin films of tetrachlorinated NDI with smaller grains. This is consistent with our findings that the interplay between kinetic

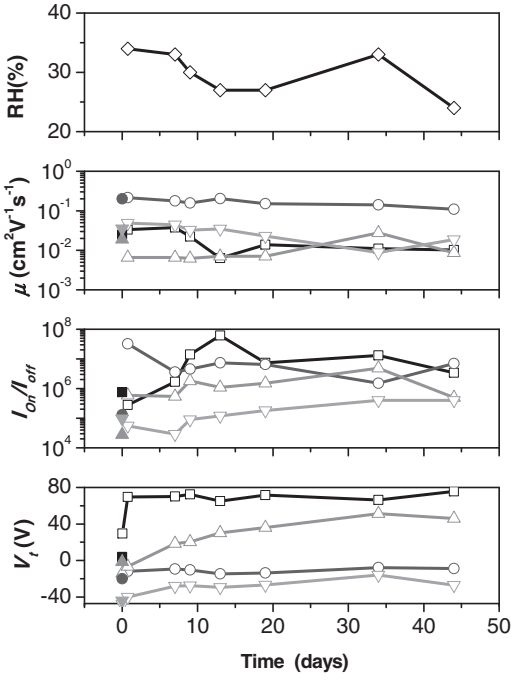

Figure 5. The air-stability testing of OTFT performance, including relative humidity (RH), mobility (μ), on/off ratio (I_{on}/I_{off}), and threshold voltage (V_t), of the SS films from **1**(square), **2** (circle), **3** (up triangle) and **4** (down triangle). The solid symbols correspond to an electrical performance in a nitrogen glove box.

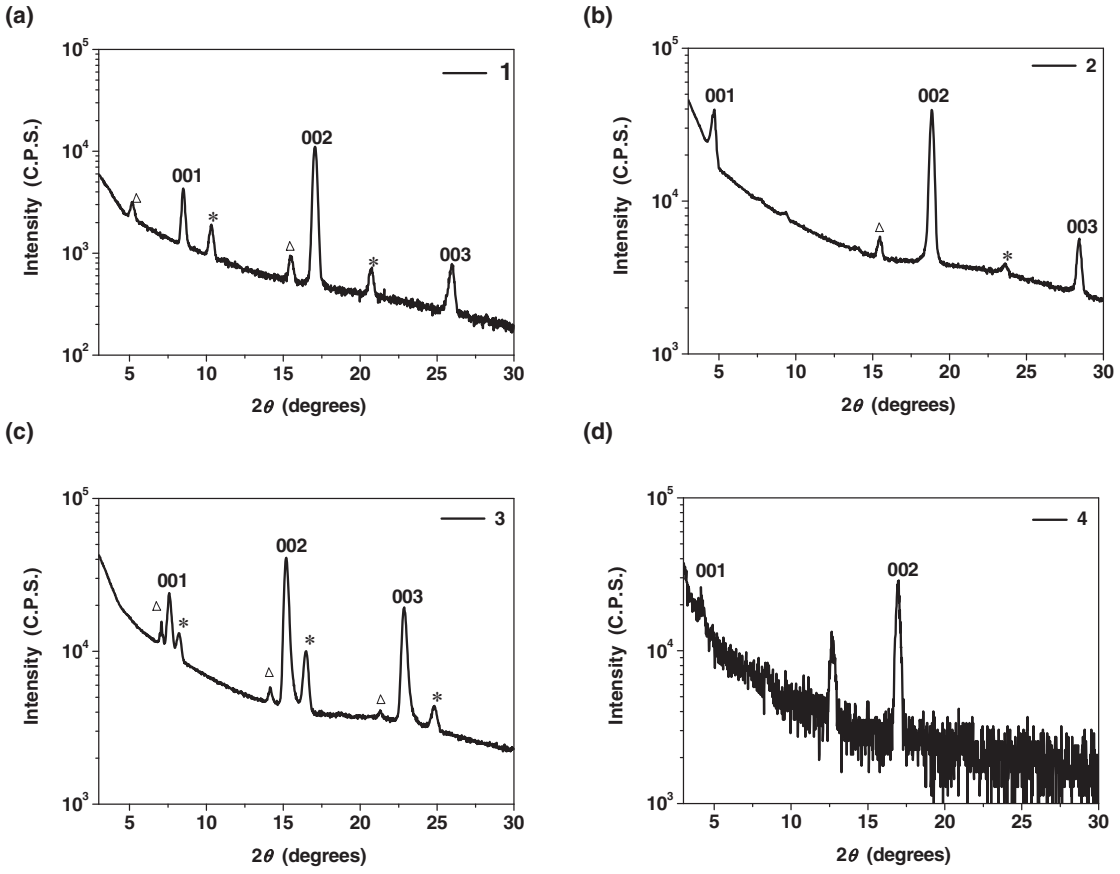

Figure 6. X-ray diffraction scans in logarithmic scale of the SS films of **1** (a), **2**, (b), **3** (c) and **4** (d). These OTFTs were fabricated in the corresponding optimized conditions. The minor phases in the thin films of **1**, **2** and **3** are marked by ∗ and.

and energetic factors plays an important role in the air-stability of n-channel OTFTs.[27] The V_t values of the dichloro-substituted NDIs OTFTs were negative, which might originate from unintentional doping.[42] It has been reported that the unintentionally doped radical anions tend to be oxidized in air,[6,42] which lowers the off current. The on/off ratios of the devices in air improved significantly by one or two orders of magnitude, as compared with those measured in an inert atmosphere. A similar observation has also been reported for fluorinated PTCDIs.[6] **2** and **4** showed positive increments of V_t from −20 V to −8 V and from −44 V to −27 V immediately after exposure to air, respectively, and did not exhibit further shift after a longer exposure. However, the V_t of **1** and **3** increased a lot in air, especially the V_t of NDI **1** increased up to +75 V. The morphology of **1** and **3** may be responsible for this large, positively-shifted V_t since many cracks on the surfaces of **1** and **3** can provide pathways for the diffusion of oxygen and moisture into the semiconductor/dielectric interface where current flow takes place.

The XRD patterns showed strong and narrow full-width at half-maximum (FWHM) peaks from the core-chlorinated NDI films, revealing the presence of highly crystalline phase in the films, as shown in **Figure 6**. The out-of-plane *d*(001)-spacing was found to be 17.08 (10.39), 18.96 (11.35), 12.49 (11.64, 10.77) and 21.33 Å for **1**, **2**, **3** and **4**, respectively, with the d-spacing for the minor phases reported in parentheses. Importantly, as compared to the d-spacings of the corresponding vapor-deposited films,[38] those of the SS thin films were slightly smaller. This is consistent with our earlier hypothesis that SS films have a different molecular tilt on the surface compared to the vacuum-evaporated films. Moreover, only one phase was observed for vapor deposited films whereas two or more phases were observed for SS films except for **4**. This result indicates that interestingly solution shearing can alter the molecular orientation in thin films. In the SS process, the shearing force at the contact line of solution and the substrate induces the growth of the crystalline films along the shearing direction. It possibly forces the semiconductors to be more tilted, decreasing the d-spacing distances. Further studies of the molecular packing of the solution-sheared and vapor-deposited thin films by grazing-incidence X-ray diffraction (GIXD) are currently underway.

3. Conclusions

We have demonstrated the electrical performance, surface morphology, and air stability of solution-sheared air-stable n-channel OTFTs based on core-chlorinated NDIs with different fluorinated side chains. The chlorination of the NDI cores improved the electron transport and air stability of the SS OTFTs. As compared to the studied NDIs, dichlorinated NDIs exhibited the highest n-channel field-effect mobility due to its less cracks and less-boundary terraced morphogy. The device of dichlorinated

NDI, **2**, showed the highest mobility of 0.57 $cm^2\ V^{-1}\ s^{-1}$ from the device with channel length direction perpendicular to the shearing direction, while only almost one third of the electron mobility was obtained along the shearing direction. The mobility anisotropy is believed to be dominated by the directions of grain boundaries (cracks). Both the introduction of electron-withdrawing chlorine groups on the NDI core (lowered LUMO) and the fluorocarbon chains (kinetic barrier for the invasion of oxygen) were helpful for improving the air-stability. The devices of dichlorinated NDIs exhibited better air-stability even after storage in air for one and a half month than that of tetrachlorinated NDI, in spite of their higher LUMO levels. This is due to the fact that the NDIs with two Cl atoms had a denser π–π stacking and terraced morphologies with less boundaries, preventing the invasion of ambient oxidant. In contrast to the OTFTs prepared through vapor-deposited thin films, the SS OTFTs of NDIs with four carbons in the fluoroalkyl chains gave the higher mobilities than those with five carbons. This may be related to the different molecular tilt angle as a result of the length of the imide side chains. We found that the solution-sheared deposition affects the molecular orientation in the crystalline thin films and slightly lowers the d-spacing distances of the small molecules, as compared with the vapor deposition. Nonetheless, the charge carrier mobility was high. This study demonstrates solution-processed n-channel core-chlorinated NDI derivatives are highly promising for low-cost large-area organic electronics.

4. Experimental Section

Characterization: Tapping-mode AFM of the films was carried out using a Multimode Nanoscope III with Extender electronics (Digital Instruments/Veeco Metrology Group, Santa Barbara, CA). A Philips PANalytical X'Pert diffractometer with a PreFIX X-ray mirror at the incident-beam side and a parallel-plate collimator at the diffracted-beam side was used to obtain diffraction patterns from thin films of the evaporated molecules. $2\theta/\omega$ scans were carried out using Cu Ka radiation at a power of 45 mV and 40 mA, with a step size of 0.02, and a step time of 1.0 s.

Transistor Device Fabrication: Highly doped *n*-type Si (100) wafers (<0.004 Ωcm) were used as substrates. A 300 nm SiO_2 layer (capacitance per unit area C_i = 10 $nFcm^{-2}$) as a gate dielectric was thermally grown onto the Si substrates. These wafers were cleaned in piranha solution, a 7:3 mixture of H_2SO_4 and H_2O_2, rinsed with deionized water, and then dried by N_2. The phenyltrichlorosilane (PTS)-treated surface on SiO_2/Si substrates were obtained by the following procedures: a clean SiO_2/Si substrate was immersed into a 3 vol% solution of phenyltrichlorosilane (PTS) in toluene at 80 °C for overnight. Then, the substrates were rinsed with toluene, acetone, isopropyl alcohol, and dried with a steam of nitrogen. The contact angle of the PTS-treated SiO_2/Si substrates measured with deionized water was approximately 70°. The organic semiconductor thin films were deposited on SiO_2/Si substrates through solution-shearing (SS) or spin-coated methods. The NDI solution was stirred at 100 °C to be fully solubilized in prior to the solution processing. Solution-sheared thin films were prepared as reported previously.[30] The solution concentrations for the SS deposition ranged from 5 to 10 $mgml^{-1}$. Spin-coated OTFT devices were prepared for comparison of performance. They were deposited from chloroform solution (5 $mgmL^{-1}$) at a spin rate of 1000 rpm for 60 s. After drying, these samples were kept overnight at 70 °C to evaporate residual solvent. Gold contacts (40 nm) were evaporated onto the SS and spin-coated thin films with a channel length (L) of 50 µm, and a channel width (w) of 1000 µm. The OTFT transfer and output characteristics were recorded in a N_2-filled glove box or in air by using a Keithley 4200 semiconductor parametric analyzer (Keithley Instruments, Cleveland, OH).

Supporting Information

Supporting Information is available from the Wiley Online Library or from the author.

Acknowledgements

This work was supported by BASF SE and. BMBF (POLYTOS project FKZ 13N10205 within leading edge cluster "Forum Organic Electronics"). W.-Y. L. acknowledges partial financial support from the National Science Council of Taiwan. Supporting Information is available online from Wiley InterScience or from the author. J.H.O. acknowledges partial financial support from 2010 Research Fund of UNIST and Basic Science Research Program through the National Research Foundation of Korea (NRF) funded by the MEST (Grant No. 2011-0026424 and Grant No. 2011-0017174).
Note: This article was amended on November 8, 2011 to correct the name of Sabin-Lucian Suraru which was incorrect in the version first published online.

Received: July 14, 2011
Revised: August 29, 2011
Published online: October 4, 2011

[1] J. Zaumseil, H. Sirringhaus, *Chem. Rev.* **2007**, *107*, 1296.
[2] Z. Bao, J. Locklin, Eds., *Organic field-effect transistors*, CRC press, Boca Raton, FL **2007**.
[3] M. Gross, D. C. Muller, H. G. Nothofer, U. Scherf, D. Neher, C. Brauchle, K. Meerholz, *Nature* **2000**, *405*, 661.
[4] R. Kroon, M. Lenes, J. C. Hummelen, P. W. M. Blom, B. De Boer, *Polym. Rev.* **2008**, *48*, 531.
[5] B. A. Jones, A. Facchetti, M. R. Wasielewski, T. J. Marks, *J. Am. Chem. Soc.* **2007**, *129*, 15259.
[6] J. H. Oh, S. Liu, Z. Bao, R. Schmidt, F. Würthner, *Appl. Phys. Lett.* **2007**, *91*, 212107.
[7] X. G. Guo, R. P. Ortiz, Y. Zheng, Y. Hu, Y. Y. Noh, K. J. Baeg, A. Facchetti, T. J. Marks, *J. Am. Chem. Soc.* **2011**, *133*, 1405.
[8] X. W. Zhan, A. Facchetti, S. Barlow, T. J. Marks, M. A. Ratner, M. R. Wasielewski, S. R. Marder, *Adv. Mater.* **2011**, *23*, 268.
[9] F. Würthner, M. Stolte, *Chem. Commun.* **2011**, *47*, 5109.
[10] X. Zhan, Z. a. Tan, B. Domercq, Z. An, X. Zhang, S. Barlow, Y. Li, D. Zhu, B. Kippelen, S. R. Marder, *J. Am. Chem. Soc.* **2007**, *129*, 7246.
[11] Z. Bao, A. J. Lovinger, J. Brown, *J. Am. Chem. Soc.* **1998**, *120*, 207.
[12] M. M. Ling, P. Erk, M. Gomez, M. Koenemann, J. Locklin, Z. N. Bao, *Adv. Mater.* **2007**, *19*, 1123.
[13] H. E. Katz, A. J. Lovinger, J. Johnson, C. Kloc, T. Siegrist, W. Li, Y. Y. Lin, A. Dodabalapur, *Nature* **2000**, *404*, 478.
[14] A. Facchetti, M. Mushrush, H. E. Katz, T. J. Marks, *Adv. Mater.* **2003**, *15*, 33.
[15] H. Yan, Z. Chen, Y. Zheng, C. Newman, J. R. Quinn, F. Dotz, M. Kastler, A. Facchetti, *Nature* **2009**, *457*, 679.
[16] R. P. Ortiz, H. Herrera, R. Blanco, H. Huang, A. Facchetti, T. J. Marks, Y. Zheng, J. L. Segura, *J. Am. Chem. Soc.* **2010**, *132*, 8440.
[17] Y. Zhao, C.-a. Di, X. Gao, Y. Hu, Y. Guo, L. Zhang, Y. Liu, J. Wang, W. Hu, D. Zhu, *Adv. Mater.* **2011**, *23*, 2448.
[18] X. K. Gao, C. A. Di, Y. B. Hu, X. D. Yang, H. Y. Fan, F. Zhang, Y. Q. Liu, H. X. Li, D. B. Zhu, *J. Am. Chem. Soc.* **2010**, *132*, 3697.
[19] Y. L. Lee, H. L. Hsu, S. Y. Chen, T. R. Yew, *J. Phys. Chem. C* **2008**, *112*, 1694.

[20] B. J. Jung, J. Sun, T. Lee, A. Sarjeant, H. E. Katz, *Chem. Mater.* **2009**, *21*, 94.
[21] B. A. Jones, A. Facchetti, T. J. Marks, M. R. Wasielewski, *Chem. Mater.* **2007**, *19*, 2703.
[22] B. A. Jones, A. Facchetti, M. R. Wasielewski, T. J. Marks, *Adv. Funct. Mater.* **2008**, *18*, 1329.
[23] D. Shukla, S. F. Nelson, D. C. Freeman, M. Rajeswaran, W. G. Ahearn, D. M. Meyer, J. T. Carey, *Chem. Mater.* **2008**, *20*, 7486.
[24] M. L. Tang, J. H. Oh, A. D. Reichardt, Z. Bao, *J. Am. Chem. Soc.* **2009**, *131*, 3733.
[25] M. Gsänger, J. H. Oh, M. Könemann, H. W. Höffken, A.-M. Krause, Z. Bao, F. Würthner, *Angew. Chem. Int. Ed.* **2010**, *49*, 740.
[26] R. Schmidt, M. M. Ling, J. H. Oh, M. Winkler, M. Konemann, Z. N. Bao, F. Würthner, *Adv. Mater.* **2007**, *19*, 3692.
[27] J. H. Oh, Y.-S. Sun, R. Schmidt, M. F. Toney, D. Nordlund, M. Könemann, F. Würthner, Z. Bao, *Chem. Mater.* **2009**, *21*, 5508.
[28] H. Yan, Z. Chen, Y. Zheng, C. Newman, J. R. Quinn, F. Dötz, M. Kastler, A. Facchetti, *Nature* **2009**, *457*, 679.
[29] Z. Chen, Y. Zheng, H. Yan, A. Facchetti, *J. Am. Chem. Soc.* **2009**, *131*, 8.
[30] H. A. Becerril, M. E. Roberts, Z. H. Liu, J. Locklin, Z. N. Bao, *Adv. Mater.* **2008**, *20*, 2588.
[31] A. Tracz, J. K. Jeszka, M. D. Watson, W. Pisula, K. Mullen, T. Pakula, *J. Am. Chem. Soc.* **2003**, *125*, 1682.
[32] W. Pisula, A. Menon, M. Stepputat, I. Lieberwirth, U. Kolb, A. Tracz, H. Sirringhaus, T. Pakula, K. Mullen, *Adv. Mater.* **2005**, *17*, 684.
[33] Z. H. Liu, H. A. Becerril, M. E. Roberts, Y. Nishi, Z. Bao, *IEEE T. Electron Dev.* **2009**, *56*, 176.
[34] J. H. Oh, W.-Y. Lee, T. Noe, W.-C. Chen, M. Könemann, Z. Bao, *J. Am. Chem. Soc.* **2011**, *133*, 4204.
[35] B. Yoo, B. A. Jones, D. Basu, D. Fine, T. Jung, S. Mohapatra, A. Facchetti, K. Dimmler, M. R. Wasielewski, T. J. Marks, A. Dodabalapur, *Adv. Mater.* **2007**, *19*, 4028.
[36] A. C. Arias, J. D. MacKenzie, I. McCulloch, J. Rivnay, A. Salleo, *Chem. Rev.* **2010**, *110*, 3.
[37] H. Sirringhaus, T. Kawase, R. H. Friend, T. Shimoda, M. Inbasekaran, W. Wu, E. P. Woo, *Science* **2000**, *290*, 2123.
[38] J. H. Oh, S.-L. Suraru, W.-Y. Lee, M. Könemann, H. W. Höffken, C. Röger, R. Schmidt, Y. Chung, W.-C. Chen, F. Würthner, Z. Bao, *Adv. Funct. Mater.* **2010**, *20*, 2148.
[39] A. Facchetti, M. Mushrush, M. H. Yoon, G. R. Hutchison, M. A. Ratner, T. J. Marks, *J. Am. Chem. Soc.* **2004**, *126*, 13859.
[40] L. H. Jimison, M. F. Toney, I. McCulloch, M. Heeney, A. Salleo, *Adv. Mater.* **2009**, *21*, 1.
[41] D. W. Li, E. J. Borkent, R. Nortrup, H. Moon, H. Katz, Z. N. Bao, *Appl. Phys. Lett.* **2005**, *86*, 042105.
[42] B. A. Jones, M. J. Ahrens, M. H. Yoon, A. Facchetti, T. J. Marks, M. R. Wasielewski, *Angew. Chem. Int. Ed.* **2004**, *43*, 6363.